Journal of Physics: Conference Series **3002** (2025) 012001 doi:10.1088/1742-6596/3002/1/012001

Nonlinear evolution in extended scalar-Gauss-Bonnet gravity

Daniela D. Doneva

Eberhard Karls University of Tübingen, Tübingen 72076, Germany

E-mail: daniela.doneva@uni-tuebingen.de

Llibert Aresté Saló

School of Mathematical Sciences, Queen Mary University of London, Mile End Road, London, E1 4NS, United Kingdom

E-mail: l.arestesalo@qmul.ac.uk

Stoytcho S. Yazadjiev

Faculty of Physics, Sofia University, Sofia 1164, Bulgaria
Institute of Mathematics and Informatics, Bulgarian Academy of Sciences, Acad. G. Bonchev St. 8, Sofia 1113, Bulgaria

E-mail: yazad@phys.uni-sofia.bg

Abstract. Scalar-Gauss-Bonnet (sGB) gravity with a coupling between the scalar field and the Ricci scalar displays interesting properties, including black hole stability, agreement with the binary pulsar constraints, and compatibility with general relativity as a cosmological late-time attractor. Previous studies have shown that spherical collapse in this framework is well-posed over a wide parameter range. Here, we extend this analysis to examine $3+1$ evolution for static and rotating black holes, confirming that the evolution remains hyperbolic if the weak coupling condition is not strongly violated. Hyperbolicity loss is linked to the gravitational sector of the physical modes, rather than the gauge choice. Our results also indicate that stationary, near-extremal scalarized black holes may exist in the Ricci-coupled sGB theory for a large enough region of the parameter space with the scalar field sourced by the spacetime curvature instead of the black hole spin.

1 Introduction

The rapid development of gravitational wave detectors promises that, in the coming decades, we will have the observational data required for precise gravity tests [1, 2, 3, 4, 5, 6, 7, 8]. Accurate theoretical gravitational waveforms, for both general relativity (GR) and its modifications, are crucial for interpreting these events. While GR waveform accuracy is steadily improving, simulations beyond GR remain under development due to two primary challenges: field equations become more complex when the GR action is modified, and well-posedness, proved in certain $3+1$ GR formulations [9, 10, 11, 12], does not necessarily apply to modified gravity [13, 14].

Scalar-Gauss-Bonnet (sGB) gravity emerged in the last two decades as an interesting and viable effective field theory model that can be very useful for examining the possible deviations from GR. One of the important properties of this theory is that black holes can support scalar hair [15, 16, 17, 18, 19], including spontaneously scalarized solutions [20, 21, 22]. Even though hyperbolicity loss is seen even in linear perturbations [23, 24], spherical symmetry allows for a hyperbolic evolution under weak coupling [25, 26]. The full $3+1$ field equations pose additional challenges, though, as the standard harmonic gauge is not well-posed [13]. A significant breakthrough showed that a modified harmonic gauge leads to well-posed $3+1$ equations for weak coupling [27, 28], enabling the development of $3+1$ numerical relativity codes [29, 30] and modified puncture gauges [31, 32].

An interesting extension of the classical sGB action is to introduce a coupling of the scalar field to the Ricci scalar [33]. This extension enables hyperbolic evolution in spherically symmetric scalar field collapse [34] and offers other important features like black hole stability and evasion of binary pulsar constraints for a certain parameter range [35]. Additionally, it addresses challenges in cosmology, allowing GR to be a cosmological late-time attractor [36]. However, early-time issues persist [37], requiring the addition of further operators to cure them [38]. In the present paper, we explore the well-posedness of Ricci-coupled sGB gravity in the $3+1$ formulation using the modified gauge proposed in [27, 28] within the puncture gauge approach [31, 32].

We follow the conventions in Wald's book [39]. Greek letters $\mu, \nu, ...$ denote spacetime indices and they run from 0 to 3; Latin letters $i, j, ...$ denote indices on the spatial hypersurfaces and they run from 1 to 3. We set $G = c = 1$.

2 Theoretical background

We consider a scalar-Gauss-Bonnet theory with a Ricci coupling having the following action

$$S = \frac{1}{16\pi}\int d^4x\sqrt{-g}\Big(R + X - \beta(\varphi)R + \frac{\lambda(\varphi)}{4}\mathcal{R}^2_{\rm GB}\Big)\,, \tag{1}$$

where R is the Ricci scalar, $\mathcal{R}^2_{\rm GB}$ is the Gauss-Bonnet invariant $\mathcal{R}^2_{\rm GB} = R^2 - 4R_{\mu\nu}R^{\mu\nu} + R_{\mu\nu\rho\sigma}R^{\mu\nu\rho\sigma}$, φ is the scalar field with a kinetic term $X = -\frac{1}{2}\nabla_\mu\varphi\nabla^\mu\varphi$ being coupled to both the Ricci scalar and the Gauss-Bonnet invariant. The coupling function $\lambda(\varphi)$ has dimensions of [length]^2 and $\beta(\phi)$ is dimensionless. Its equations of motion yield

$$(1-\beta(\varphi))(R_{\mu\nu} - \frac{1}{2}Rg_{\mu\nu}) + \Gamma_{\mu\nu} = \frac{1}{2}\nabla_\mu\varphi\nabla_\nu\varphi - \frac{1}{4}g_{\mu\nu}\nabla_\alpha\varphi\nabla^\alpha\varphi + (g_{\mu\nu}\Box - \nabla_\mu\nabla_\nu)\beta(\varphi)\,, \tag{2a}$$

$$\nabla_\alpha\nabla^\alpha\varphi = -\frac{\lambda'(\varphi)}{4}\mathcal{R}^2_{GB} + \beta'(\varphi)R\,, \tag{2b}$$

where $\Gamma_{\mu\nu}$ is defined as

$$\Gamma_{\mu\nu} \;=\; -\frac{1}{2}R\Omega_{\mu\nu} - \Omega_\alpha{}^\alpha\left(R_{\mu\nu} - \frac{1}{2}Rg_{\mu\nu}\right) + 2\,R_{\alpha(\mu}\Omega_{\nu)}{}^\alpha - g_{\mu\nu}R^{\alpha\beta}\Omega_{\alpha\beta} + R^\beta_{\mu\alpha\nu}\Omega_\beta{}^\alpha\,, \tag{3}$$

with $\Omega_{\mu\nu} = \nabla_\mu\nabla_\nu\,\lambda(\varphi)$.

For the numerical solution of the above field equations we use the modified CCZ4 formalism introduced by [28, 27, 31, 32]. More detail on that, including the explicit form of the evolution equations for the $3+1$ formalism can be found in [40].

The coupling functions $\lambda(\varphi)$ and $\beta(\varphi)$ we will work with are the following

$$\lambda(\varphi) \;=\; \lambda_{\rm GB}\,\varphi^2\,, \tag{4}$$

$$\beta(\varphi) \;=\; \beta_{\rm Ricc}\,\varphi^2\,. \tag{5}$$

This choice is motivated by the fact that it allows the so-called spontaneous scalarization [41, 20, 21, 22]. Therefore, the weak field limit coincides with Einstein's gravity while for strong enough spacetime curvature a Kerr black hole destabilizes, giving rise to a black hole with scalar hair. A pure φ^2 term in (4) will lead to scalarized but unstable black hole solutions. For large enough $\beta_{\rm Ricc}$, though, the resulting black hole solutions are linearly stable [33] similar to the introduction of higher order in φ terms in the $\lambda(\varphi)$ coupling [20, 42, 43].

2.1 Effective metric

The equations of motion remain hyperbolic if their principal part is diagonalizable with real eigenvalues and a complete, linearly independent set of bounded eigenvectors that vary smoothly. The gauge sector eigenvalues lie on the null cones of the auxiliary metrics (which are introduced in the modified harmonic gauge [28, 27]), while the physical sector is governed by a degree-6 characteristic polynomial, which factorizes into quadratic and quartic polynomials [44]. The quadratic polynomial, defined by an "effective metric," corresponds to "purely gravitational" polarizations, whereas the quartic one generally involves both gravitational and scalar field polarizations.

Although the quartic polynomial represents the "fastest" degrees of freedom [44], hyperbolicity loss does not necessarily occur there, and it is challenging to analyze hyperbolicity in that sector. Thus, we focus on "purely gravitational" polarizations, which align with observed simulation breakdowns in our previous findings [45]. Nevertheless, non-hyperbolic behavior may also arise from the quartic polynomial eigenvalues.

In the Ricci-coupled sGB theory, the effective metric yields

$$g^{\mu\nu}_{\rm eff} = g^{\mu\nu}(1-\beta(\varphi)) - \Omega^{\mu\nu}\,, \tag{6}$$

and its determinant, normalized to the GR value, can be expressed as

$$\begin{aligned}\frac{\det(g^{\mu\nu}_{\rm eff})}{\det(g^{\mu\nu})} &= \left(\tfrac{1}{1+\Omega^{\perp\perp}-\beta(\varphi)}\right)^2 \det\Big\{\tfrac{1}{\chi}\big[(\gamma^{ij}(1-\beta(\varphi))-\Omega^{ij})(1+\Omega^{\perp\perp}-\beta(\varphi)) - \tfrac{2}{\alpha}\Omega^{\perp(i}\beta^{j)} \\ &\qquad -(1-\beta(\varphi))\Omega^{\perp\perp}\tfrac{\beta^i\beta^j}{\alpha^2} + \Omega^{\perp i}\Omega^{\perp j}\big]\Big\}\,,\end{aligned} \tag{7}$$

where $\Omega^{ij} = \gamma^i_\mu\gamma^j_\nu\Omega^{\mu\nu}$, $\Omega^{\perp i} = -n_\mu\gamma^i_\nu\Omega^{\mu\nu}$ and $\Omega^{\perp\perp} = n_\mu n_\nu\Omega^{\mu\nu}$. In the results shown later, we will consider the normalized determinant

$$G_{\rm eff} \equiv (1+\Omega^{\perp\perp}-\beta(\varphi))^2\,\frac{\det(g^{\mu\nu}_{\rm eff})}{\det(g^{\mu\nu})}\,, \tag{8}$$

which has no divergences when hyperbolicity is lost. It is also normalized to unity when no scalar field is present.

2.2 Weak coupling condition

sGB can be viewed as an effective field theory (EFT) that arises as a low energy limit of a more fundamental theory. In order for our theory to be justified and valid as an EFT, though, one has to make sure that we are not beyond the threshold where the EFT breaks down and the higher derivative terms become relevant. This is ensured as long as, throughout its evolution, the theory is in the weak coupling regime. This yields the following Weak Coupling Condition (WCC), [32, 45]:

$$\sqrt{|\lambda'(\varphi)|}/L \ll 1\,. \tag{9}$$

Here L is the inverse of the shortest physical length scale characterizing the system, defined as

$$L^{-1} = \max\{|R_{ij}|^{1/2}, |\nabla_\mu\varphi|, |\nabla_\mu\nabla_\nu\varphi|^{1/2}, |\mathcal{R}^2_{\rm GB}|^{1/4}\}\,. \tag{10}$$

3 Results

3.1 Numerical set-up and hyperbolicity loss treatment

The work [34] demonstrated that $1+1$ non-linear evolution in Ricci-coupled sGB theory remains hyperbolic across a wide parameter space. Extending this analysis to $3+1$ evolution presents an important and natural, although complicated, next step and it is the focus of the present paper. Another important

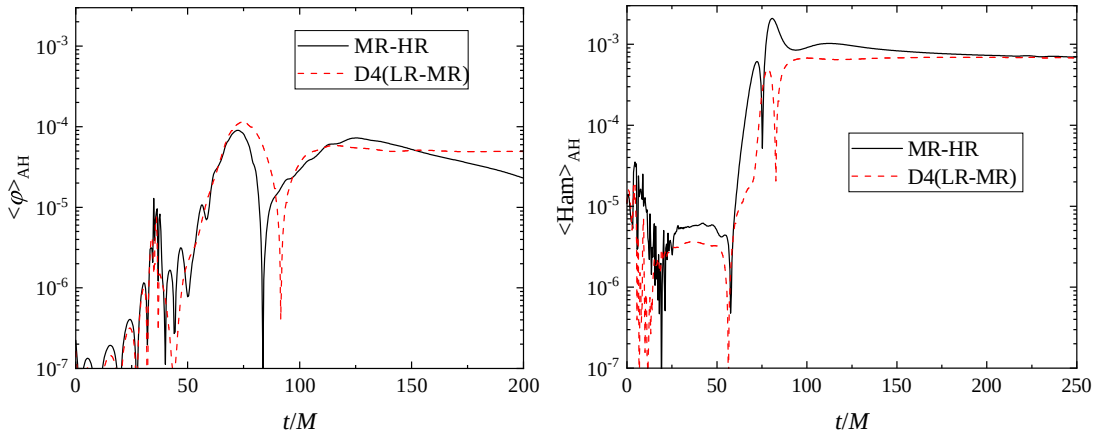

Figure 1: The difference between the scalar field and Hamiltonian constraint evolution performed for three different resolutions for $\lambda_{\rm GB}/M^2 = 6$, $\gamma_{\rm GB} = 0$, and $\beta_{\rm Ricc} = 10$. The three resolutions are chosen to have 96 (low resolution), 128 (medium resolution), and 160 (high resolution) points at the coarser level in each spatial direction, with 6 refinement levels, and a domain size of $256M$. The difference between low and medium resolution (red dashed line) is multiplied by the fourth-order convergence factor $D_4 = \frac{h^4_{\rm LR} - h^4_{\rm ML}}{h^4_{\rm MR} - h^4_{\rm HR}}$. (*left panel*) The average value of the scalar field at the apparent horizon. (*right panel*) The average value of the Hamiltonian constraint at the horizon.

difference with respect to [34] is that they investigate scalar cloud collapse, while we evolve an unstable Kerr black hole which scalarizes during the evolution.

By employing a modified puncture gauge for sGB gravity [27, 28, 31, 32], we hypothesize that hyperbolicity loss, at least for the simulations performed, is tied to the physical modes of the purely gravitational sector, rather than the mixed scalar-gravitational sector, in a similar way to sGB gravity [44]. This is indicated by the determinant of the effective metric (8), which turns negative shortly before the simulation fails, suggesting that the mode speeds may either diverge or become degenerate [44, 45]. Below we argue, though, that hyperbolicity is preserved when the weak coupling condition is satisfied and in the limiting case – even slightly violated [45]. For that purpose we employ a newly developed modification of `GRFolres` [46] (based on `GRChombo` [47, 48, 49]), that was implemented taking into account the Ricci scalar coupling in eqs. (2). More details about the code can be found in [40]. The chosen resolution is 128 points in each spatial direction with 6 refinement levels and a domain size of $256M$.

Our initial data is an unstable Kerr black hole (with respect to scalar field perturbations). On top of it we superimpose a Gaussian scalar field pulse with a marginal amplitude located at roughly $20M$ outside the black hole horizon. Triggered by the scalar field pulse, scalar hair starts developing around the black hole. More specifically, the scalar field grows exponentially either until it reaches equilibrium or a loss of hyperbolicity occurs. Such loss of hyperbolicity typically arises first within the black hole horizon and can later extend beyond it [50, 51, 52]. As long as this non-hyperbolic region remains confined within the horizon, it remains causally disconnected from the rest of spacetime and it can be still accepted as a viable black hole solution. However, from a numerical perspective, any elliptic region within the computational domain leads to unavoidable numerical instabilities and thus a code crash. Consequently, to pinpoint the boundary between hyperbolic and non-hyperbolic solutions outside the apparent horizon, it is advantageous to turn off the Gauss-Bonnet coupling inside the black hole and slowly turn it on as the horizon is approached. Since this "change" of the field equations happens only inside the horizon, it does not affect the black hole dynamics outside the horizon. The procedure and its viability are described in detail in [31, 32, 40].

As evidence for the validity of the developed numerical relativity code, a convergence test is presented in Fig. 1, where the time evolution of the scalar field at the black hole horizon and the Hamiltonian constrain are displayed for three different resolutions. We observe that the convergence matches well to a fourth-order as expected.

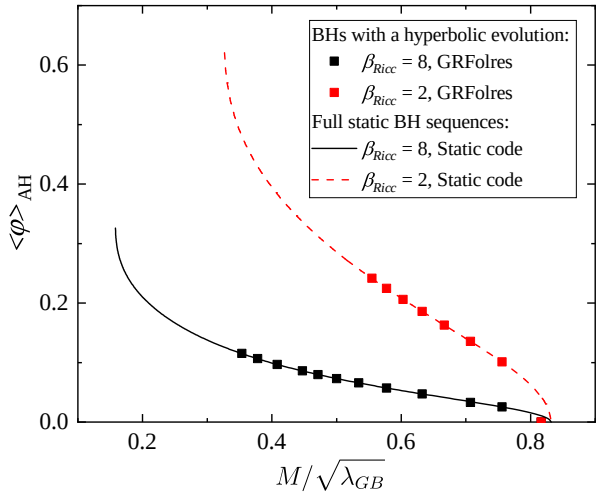

Figure 2: The mean value of the scalar field at the apparent horizon $\langle\varphi\rangle_{\rm AH}$ as a function of the normalized black hole mass $M/\sqrt{\lambda_{\rm GB}}$ for sequences of black holes with $\gamma_{\rm GB} = 0$ and two different values of the Ricci coupling constant $\beta_{\rm Ricc} = 2$ and $\beta_{\rm Ricc} = 8$. The squares are the end states of the $3 + 1$ simulations of black hole scalarization while the lines depict the full sequence of solutions obtained through solving the static field equations. The sequences of red and black squares are terminated at the last model for which we were able to perform hyperbolic evolution, since black hole evolutions with lower $M/\sqrt{\lambda_{\rm GB}}$ develop hyperbolicity loss during the scalar field growth.

3.2 Hyperbolicity of black hole non-linear evolution in Ricci-coupled sGB theory

We first present results for the evolution of non-rotating black hole sequences with increasing mass. Two values of the Ricci coupling constant, $\beta_{\rm Ricc}$, are chosen and they both ensure that the resulting static black holes are linearly stable. The mass and scalar field at the black hole horizon, shown in Fig. 3, represent the end states of the numerical simulations after the black hole scalarization has settled to a quasi-stationary solution. The red and black squares correspond to the two values of $\beta_{\rm Ricc}$. Only hyperbolic evolutions are shown, as for the rest of the simulations (with a higher scalar charge and lower mass) hyperbolicity is lost early in scalar field development [45]. As Fig. 3 illustrates, higher scalar fields at the horizon (before hyperbolicity loss) are achievable with the smaller value $\beta_{\rm Ricc} = 2$. Conversely, increasing $\beta_{\rm Ricc}$ broadens the range of $M/\sqrt{\lambda_{\rm GB}}$ for stable evolution, consistent with spherical symmetry findings [34].

For comparison, Fig. 3 also includes solid and dashed lines representing static field equation solutions employing a modification of the 1D code developed in [20]. These lines depict all regular, asymptotically flat, and linearly stable black hole solutions, irrespective of hyperbolicity. The lines originate from $\langle\varphi\rangle_{\rm AH} = 0$ at the GR bifurcation point and end at smaller $M/\sqrt{\lambda_{\rm GB}}$. The close agreement between lines and points confirms the accuracy of the `GRFolres` extension. The static solutions span a wider range of $M/\sqrt{\lambda_{\rm GB}}$ than the models from non-linear evolution, as black holes with larger $\langle\varphi\rangle_{\rm AH}$ cannot form dynamically through hyperbolic evolution. Similar to pure sGB gravity [45], only small scalar field solutions are hyperbolic.

Note that hyperbolicity depends on both the final black hole state and the path to this configuration. In Fig. 3, we start from GR initial data that, due to coupling function and parameters choice, leads to scalar field growth as the black hole is unstable under scalar field perturbations. Starting from constraint-satisfying scalarized black hole initial data would likely prevent the rapid scalar field growth, possibly preserving hyperbolicity over a broader parameter range.

To understand hyperbolicity loss, let us examine a single black hole's evolution. Fig. 6 shows snapshots of the scalar field evolution (top panel) and the normalized determinant of the effective metric, $G_{\rm eff}$ eq. (8) (lower panel). The first snapshot shows the scalar field as it begins to develop, and the last one captures the step just before the code crashes. In the $G_{\rm eff}$ plots, black areas indicate negative values, signaling hyperbolicity loss. Inside the black hole horizon (marked by a dashed white line), the Gauss-Bonnet coupling is turned off, with $\lambda(\varphi) = 0$ and $\beta(\varphi) = 0$ near the singularity, as detailed above. That is why it is satisfied that $G_{\rm eff} = 1$ there. The coupling is completely reactivated within the horizon,

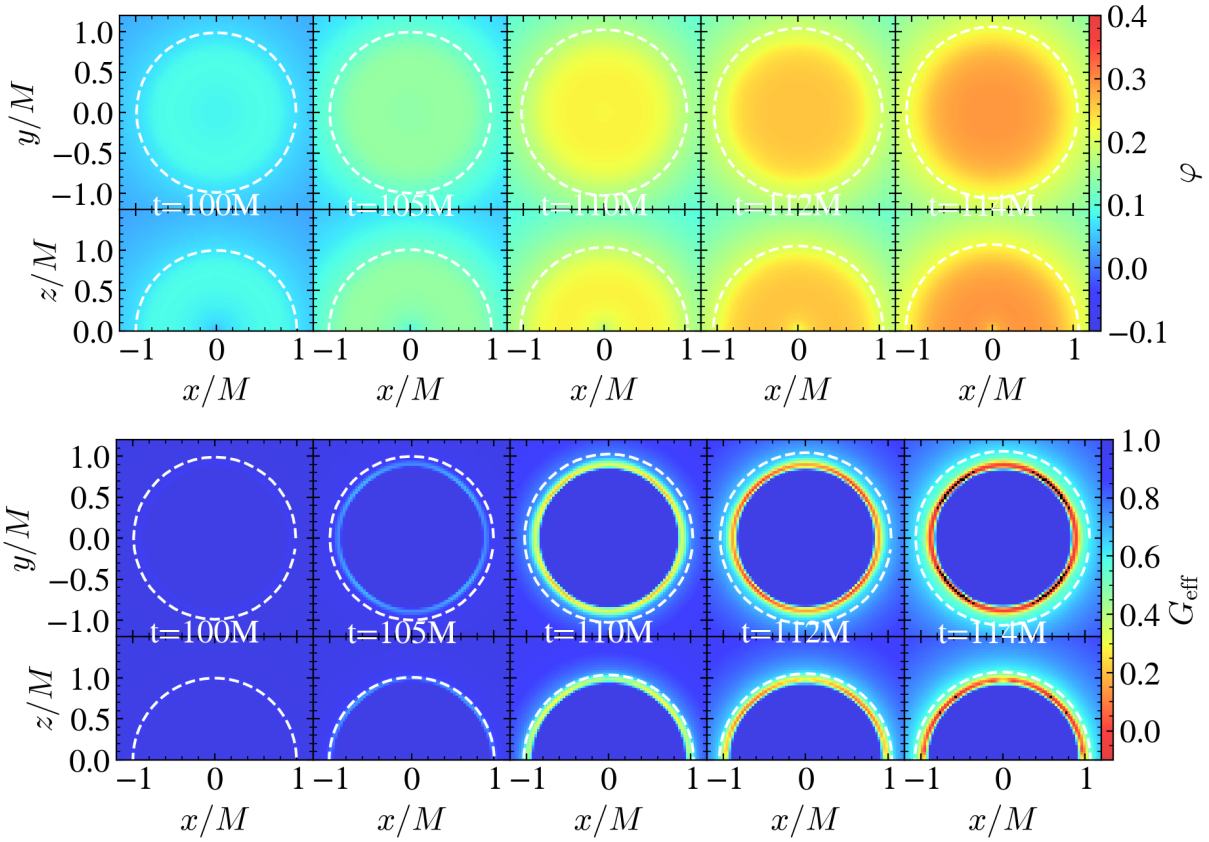

Figure 3: Time evolution of a non-rotating black hole with $\lambda_{\rm GB}/M^2 = 4$, $\gamma_{\rm GB} = 0$, $\beta_{\rm Ricc} = 2$. Several coordinate times during the scalarization are plotted, capturing the evolution just before the code breaks down due to a loss of hyperbolicity. Note that the time frames are not equally spaced to better demonstrate the development of a negative $G_{\rm eff}$ region. In each figure, both $x-y$ and $x-z$ slices are depicted. The apparent horizon is plotted as a white dashed line. *(top)* Time evolution of the scalar field. *(bottom)* Time evolution of the normalized determinant of the effective metric $G_{\rm eff}$ defined by eq. (8). Negative values of $G_{\rm eff}$ are depicted in black.

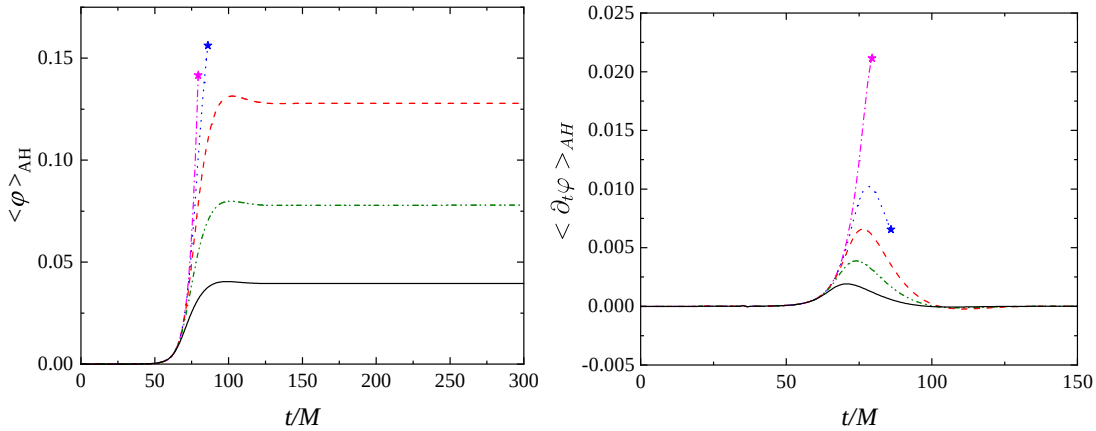

Figure 4: The *left figures* depict the scalar field evolution for both hyperbolic and non-hyperbolic black hole evolutions. The time derivative of the scalar field is presented in the *right figures*. Stars indicate the moment of the evolution when hyperbolicity is lost, which typically happens when the scalar field starts growing during spontaneous scalarization.

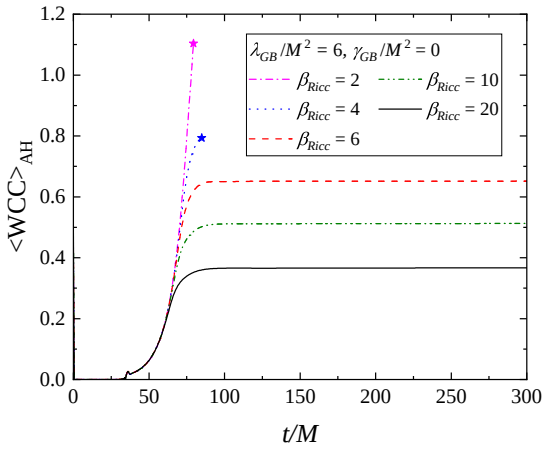

Figure 5: The evolution of the weak coupling condition defined by eq. (9) for the same models as in Fig. 4.

preventing deviations from the true solution outside the black hole [31, 32].

The primary observation is the formation of a $G_{\rm eff} < 0$ (black) region just before the code halts, strongly indicating that the code failure is due to hyperbolicity loss in the gravitational sector governed by the effective metric (8). Like pure sGB gravity, this most probably cannot be resolved by gauge changes.

In Figs. 4 and 5 we plot the time evolution of the scalar field, its time derivative and the weak coupling condition defined by (9) for models with fixed $M/\sqrt{\lambda_{\rm GB}}$. The simulations are performed for non-rotating black holes where $\beta_{\rm Ricc}$ varies. The range of $\beta_{\rm Ricc}$ is chosen on the threshold of hyperbolicity loss. A star at the end of some lines marks hyperbolicity loss while for the rest we observe a saturation of the scalar field to a constant. Interestingly, even though the non-hyperbolic model can reach a larger scalar field before the code breaks down, its time derivative is actually smaller. This is another evidence that the loss of hyperbolicity is strongly affected by the gradients of the metric potentials and the scalar field and, therefore, it is affected by the initial data choice.

The weak coupling condition in Fig. 5 has an oscillatory behavior at early times, which is an artifact of the changes in the scalar field gradient before it settles to an equilibrium value. Clearly, one can go slightly beyond the weak coupling condition while still maintaining hyperbolicity since the weak coupling condition reaches the order of unity before hyperbolicity is lost.

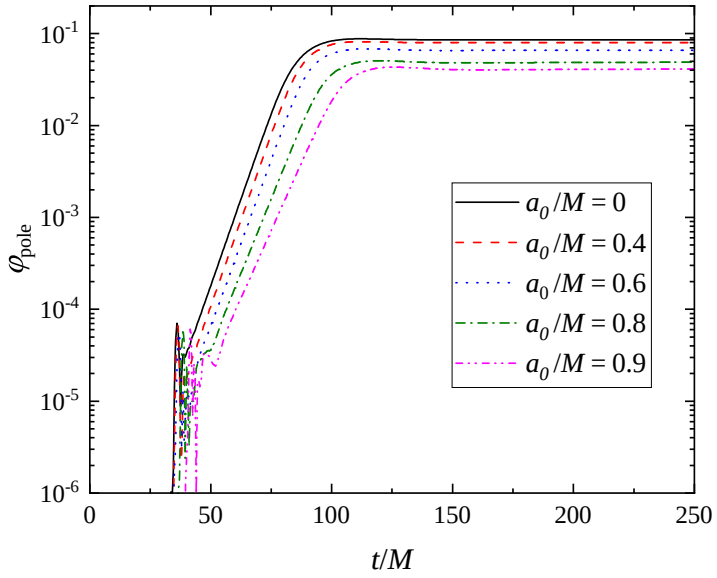

Figure 6: The scalar field on the pole for models with increasing angular momentum a_0/M, having $M/\sqrt{\lambda_{\rm GB}} = 0.45$, $\gamma_{\rm GB} = 0$ and $\beta_{\rm Ricc} = 8$.

3.3 Rotating black holes with Ricci scalar coupling

A key question is whether hyperbolicity is preserved for the models in the previous section when rotation is included. To explore this, we selected as initial data a black hole model near hyperbolicity loss in Fig. 2 and evolved it with gradually increasing black hole angular momentum. The scalar field evolution at the horizon, presented in Fig. 6, indicates stable (thus hyperbolic) evolution even for high rotation rates. We could have a stable, well-behaved evolution as high as $a_0/M = 0.9$. If one gets closer to the extremal limit then stable evolution requires fine-tuning of the auxiliary simulation parameters associated to the gauge and the CCZ4 numerical dampings [31, 32].

4 Conclusions

In this paper, we investigated the $3 + 1$ non-linear evolution of static and rotating black holes in scalar-Gauss-Bonnet (sGB) gravity, incorporating an additional coupling between the scalar field and the Ricci scalar. To achieve this, we developed a modified version of the `GRFolres` code, based on `GRChombo`, to enable a self-consistent coupled evolution of the field equations.

Our results show that, in line with mathematical analysis, the modified gauge developed in sGB gravity [27, 28, 31] leads to hyperbolic evolution with the addition of a Ricci coupling, as long as the weak coupling condition is met. Interestingly, well-posedness is numerically maintained even slightly above the threshold where the weak coupling condition is violated for both static and rotating black holes. As a notable outcome, we found that rotating black holes with a scalar field sourced by the spacetime curvature can exist at high angular momenta, close to the extremal limit. This contrasts with prior studies [53] in sGB gravity, where the domain for black hole existence narrowed significantly near the extremal limit due to regularity condition violations at the horizon. Our results suggest that with an appropriate choice of coupling between the scalar field and the Gauss-Bonnet invariant, similar near-extremal scalarized black holes with a non-negligible scalar field may also exist in pure sGB gravity. A systematic study of stationary solutions in this context is ongoing.

It is also interesting to compare the thresholds of hyperbolicity loss in Ricci-coupled sGB theory and in sGB gravity with a more sophisticated coupling function that includes both quadratic and quartic scalar field terms. This alternative coupling also stabilizes the scalarized solution, even without a Ricci coupling. Based on previous studies [40], we can confirm that while these theories are distinct, the thresholds for hyperbolicity loss in terms of scalar field strength and weak coupling condition violations are similar. Therefore, it will be interesting to explore how future observations, such as gravitational waves from black hole mergers, could potentially distinguish between these two cases.

Acknowledgements
This study is in part financed by the European Union-NextGenerationEU, through the National Recovery and Resilience Plan of the Republic of Bulgaria, project No. BG-RRP-2.004-0008-C01. DD acknowledges financial support via an Emmy Noether Research Group funded by the German Research Foundation (DFG) under grant no. DO 1771/1-1. LAS is supported by an LMS Early Career Fellowship. We acknowledge Discoverer PetaSC and EuroHPC JU for awarding this project access to Discoverer supercomputer resources. We thank the entire `GRChombo` [1] collaboration for their support and code development work.

References

[1] Abbott B P *et al.* (LIGO Scientific, Virgo) 2016 *Phys. Rev. Lett.* **116** 221101 [Erratum: Phys.Rev.Lett. 121, 129902 (2018)] (*Preprint* `1602.03841`)

[2] Abbott B P *et al.* (LIGO Scientific, Virgo) 2019 *Phys. Rev. Lett.* **123** 011102 (*Preprint* `1811.00364`)

[3] Abbott B P *et al.* (LIGO Scientific, Virgo) 2019 *Phys. Rev. D* **100** 104036 (*Preprint* `1903.04467`)

[4] Abbott R *et al.* (LIGO Scientific, Virgo) 2021 *Phys. Rev. D* **103** 122002 (*Preprint* `2010.14529`)

[5] Abbott R *et al.* (LIGO Scientific, VIRGO, KAGRA) 2021 (*Preprint* `2112.06861`)

[6] Yunes N, Yagi K and Pretorius F 2016 *Phys. Rev. D* **94** 084002 (*Preprint* `1603.08955`)

[7] Arun K G *et al.* (LISA) 2022 *Living Rev. Rel.* **25** 4 (*Preprint* `2205.01597`)

[8] Barack L *et al.* 2019 *Class. Quant. Grav.* **36** 143001 (*Preprint* `1806.05195`)

[9] Bruhat Y 1962 The cauchy problem *Gravitation: an introduction to current research* ed Witten L (John Wiley and Sons)

[10] Sarbach O, Calabrese G, Pullin J and Tiglio M 2002 *Phys. Rev. D* **66** 064002 (*Preprint* `gr-qc/0205064`)

[11] Beyer H R and Sarbach O 2004 *Phys. Rev. D* **70** 104004 (*Preprint* `gr-qc/0406003`)

[12] Reula O A 2004 *J. Hyperbol. Diff. Equat.* **1** 251–269 (*Preprint* `gr-qc/0403007`)

[13] Papallo G and Reall H S 2017 *Phys. Rev. D* **96** 044019 (*Preprint* `1705.04370`)

[14] Bernard L, Lehner L and Luna R 2019 *Phys. Rev. D* **100** 024011 (*Preprint* `1904.12866`)

[15] Mignemi S and Stewart N R 1993 *Phys. Rev. D* **47** 5259–5269 (*Preprint* `hep-th/9212146`)

[16] Kanti P, Mavromatos N E, Rizos J, Tamvakis K and Winstanley E 1996 *Phys. Rev. D* **54** 5049–5058 (*Preprint* `hep-th/9511071`)

[17] Torii T, Yajima H and Maeda K i 1997 *Phys. Rev. D* **55** 739–753 (*Preprint* `gr-qc/9606034`)

[18] Pani P and Cardoso V 2009 *Phys. Rev. D* **79** 084031 (*Preprint* `0902.1569`)

[19] Sotiriou T P and Zhou S Y 2014 *Phys. Rev. Lett.* **112** 251102 (*Preprint* `1312.3622`)

[20] Doneva D D and Yazadjiev S S 2018 *Phys. Rev. Lett.* **120** 131103 (*Preprint* `1711.01187`)

[21] Silva H O, Sakstein J, Gualtieri L, Sotiriou T P and Berti E 2018 *Phys. Rev. Lett.* **120** 131104 (*Preprint* `1711.02080`)

[22] Antoniou G, Bakopoulos A and Kanti P 2018 *Phys. Rev. Lett.* **120** 131102 (*Preprint* `1711.03390`)

[23] Blázquez-Salcedo J L, Doneva D D, Kunz J and Yazadjiev S S 2018 *Phys. Rev. D* **98** 084011 (*Preprint* `1805.05755`)

[24] Blázquez-Salcedo J L, Doneva D D, Kahlen S, Kunz J, Nedkova P and Yazadjiev S S 2020 *Phys. Rev. D* **101** 104006 (*Preprint* `2003.02862`)

[1] `www.grchombo.org`

[25] Ripley J L and Pretorius F 2019 *Phys. Rev. D* **99** 084014 (*Preprint* 1902.01468)

[26] R A H K, Ripley J L and Yunes N 2023 *Phys. Rev. D* **107** 044044 (*Preprint* 2211.08477)

[27] Kovács A D and Reall H S 2020 *Phys. Rev. Lett.* **124** 221101 (*Preprint* 2003.04327)

[28] Kovács A D and Reall H S 2020 *Phys. Rev. D* **101** 124003 (*Preprint* 2003.08398)

[29] East W E and Ripley J L 2021 *Phys. Rev. Lett.* **127** 101102 (*Preprint* 2105.08571)

[30] Corman M, Ripley J L and East W E 2023 *Phys. Rev. D* **107** 024014 (*Preprint* 2210.09235)

[31] Aresté Saló L, Clough K and Figueras P 2022 *Phys. Rev. Lett.* **129** 261104 (*Preprint* 2208.14470)

[32] Aresté Saló L, Clough K and Figueras P 2023 *Phys. Rev. D* **108** 084018 (*Preprint* 2306.14966)

[33] Antoniou G, Lehébel A, Ventagli G and Sotiriou T P 2021 *Phys. Rev. D* **104** 044002 (*Preprint* 2105.04479)

[34] Thaalba F, Bezares M, Franchini N and Sotiriou T P 2024 *Phys. Rev. D* **109** L041503 (*Preprint* 2306.01695)

[35] Ventagli G, Antoniou G, Lehébel A and Sotiriou T P 2021 *Phys. Rev. D* **104** 124078 (*Preprint* 2111.03644)

[36] Antoniou G, Bordin L and Sotiriou T P 2021 *Phys. Rev. D* **103** 024012 (*Preprint* 2004.14985)

[37] Anson T, Babichev E, Charmousis C and Ramazanov S 2019 *JCAP* **06** 023 (*Preprint* 1903.02399)

[38] Babichev E, Sawicki I and Trombetta L G 2024 (*Preprint* 2403.15537)

[39] Wald R M 1984 *General Relativity* (Chicago, USA: Chicago Univ. Pr.)

[40] Doneva D D, Aresté Saló L and Yazadjiev S S 2024 *Phys. Rev. D* **110** 024040 (*Preprint* 2404.15526)

[41] Doneva D D, Ramazanoğlu F M, Silva H O, Sotiriou T P and Yazadjiev S S 2024 *Rev. Mod. Phys.* **96** 015004 (*Preprint* 2211.01766)

[42] Minamitsuji M and Ikeda T 2019 *Phys. Rev. D* **99** 044017 (*Preprint* 1812.03551)

[43] Silva H O, Macedo C F B, Sotiriou T P, Gualtieri L, Sakstein J and Berti E 2019 *Phys. Rev. D* **99** 064011 (*Preprint* 1812.05590)

[44] Reall H S 2021 *Phys. Rev. D* **103** 084027 (*Preprint* 2101.11623)

[45] Doneva D D, Aresté Saló L, Clough K, Figueras P and Yazadjiev S S 2023 *Phys. Rev. D* **108** 084017 (*Preprint* 2307.06474)

[46] Aresté Saló L, Brady S E, Clough K, Doneva D, Evstafyeva T, Figueras P, França T, Rossi L and Yao S 2023 (*Preprint* 2309.06225)

[47] Clough K, Figueras P, Finkel H, Kunesch M, Lim E A and Tunyasuvunakool S 2015 *Class. Quant. Grav.* **32** 245011 (*Preprint* 1503.03436)

[48] Andrade T *et al.* 2021 *J. Open Source Softw.* **6** 3703 (*Preprint* 2201.03458)

[49] Radia M, Sperhake U, Drew A, Clough K, Figueras P, Lim E A, Ripley J L, Aurrekoetxea J C, França T and Helfer T 2022 *Class. Quant. Grav.* **39** 135006 (*Preprint* 2112.10567)

[50] Ripley J L and Pretorius F 2020 *Phys. Rev. D* **101** 044015 (*Preprint* 1911.11027)

[51] Ripley J L and Pretorius F 2020 *Class. Quant. Grav.* **37** 155003 (*Preprint* 2005.05417)

[52] Corelli F, De Amicis M, Ikeda T and Pani P 2023 *Phys. Rev. Lett.* **130** 091501 (*Preprint* 2205.13006)

[53] Cunha P V P, Herdeiro C A R and Radu E 2019 *Phys. Rev. Lett.* **123** 011101 (*Preprint* 1904.09997)